



Comprehensive strength deterioration model of compacted loess exposed to drying–wetting cycles

Chang-ming Hu¹ · Yi-li Yuan¹ · Yuan Mei¹ · Xue-yan Wang^{1,2} · Zheng Liu¹

Received: 31 January 2019 / Accepted: 4 June 2019 / Published online: 15 June 2019
© Springer-Verlag GmbH Germany, part of Springer Nature 2019

Abstract

The strength deterioration of compacted loess caused by drying–wetting cycles is influenced by various factors. In this paper, the influence of dry density (ρ), drying–wetting amplitude (A), and lower bounds of drying–wetting cycles (w_l) on strength deterioration of compacted loess due to drying–wetting cycles was studied through triaxial tests and environmental scanning electron microscope (ESEM). By fitting a hyperbolic function to the deterioration data, the influence of ρ , A , and w_l on the maximum deterioration rate and the development speed of the deterioration of strength parameters were quantitatively analyzed. Accordingly, a compacted loess deterioration model (CLDM) that comprehensively considers the influencing factors was established. Finally, based on Python, the CLDM was applied to finite element software ABAQUS, and the stability of a loess fill slope after exposure to drying–wetting cycles was analyzed. Analysis results show that the CLDM is capable of simulating the effect of drying–wetting cycles on the stability of fill slopes.

Keywords Drying–wetting cycles · Compacted loess · Strength deterioration · Deterioration model · Finite element method

Introduction

Loess is widely distributed in many regions, such as Western America, Southern Russia, Northern France, Canada, Australia, Middle East, Western Europe, and Northwestern China (Taylor et al. 1983). Over the last decade, many loess high fill projects have been constructed in the loess area of Northwestern China. Collapsibility of loess can be eliminated by dense compaction. However, its strong water sensitivity, and cyclic water content changes, i.e., drying–wetting (D–W) cycles, may affect the shear strength of fine-compacted loess and thus influence the stability of a fill slope and embankment constructed from compacted loess (Allam and Sridharan 1981; Clarke and Smethurst 2010; Li et al. 2018).

D–W cycles caused by environmental factors such as rainfall, groundwater table changes, and surface evaporation

change the microstructure of the soil, thus affecting the physical and mechanical behavior of soils in different ways (Nowamooz and Masrouri 2010; Aldaood et al. 2014). Numerous studies have focused on this issue in order to understand the influence of D–W cycles on different soils. By comparing the influence of D–W cycles and freeze–thaw cycles on compacted loess, Li et al. (2018) suggested that D–W cycles have more significant weathering effects on compacted loess, and collapsibility reappears after a few D–W cycles. The structural strength of compacted loess degrades when subjected to D–W cycles (Yuan et al. 2017). D–W cycles irreversibly affect the deformation characteristics of compacted loess, and the relationship between D–W cycles and the secant modulus of compacted loess is exponential (Wang et al. 2016a, b). Many studies focused on other soils, including swelling soil (Rayhani et al. 2007; Wu et al. 2012; Estabragh et al. 2013; Kampala et al. 2013; Roshani et al. 2018), residual soil (Rao and Revanasiddappa 2006; Md et al. 2016), clay and silty clay (Rayhani et al. 2008; Guan et al. 2009; Chen and Ng 2013; Aldaood et al. 2014), and laterite soil (Benatti et al. 2011; Kholghifard et al. 2014). Existing research suggests that D–W cycles influence the physical and mechanical properties of soils, including compacted loess. Shear strength deterioration in soils (Pires et al. 2005; Tang et al. 2011) caused by D–W cycles may

✉ Yi-li Yuan
Yuan.xauat@qq.com

¹ College of Civil Engineering, Xi'an University of Architecture and Technology, Xi'an 710055, Shaanxi, China

² College of Urban Planning and Municipal Engineering, Xi'an Polytechnic University, Xi'an 710048, Shaanxi, China

reduce the stability of the geotechnical structures like fill slopes and embankments, which is a concern in practical engineering (Al-Obaydi et al. 2010; Al-Zubaydi 2011). In order to study the relationship between strength parameters and D–W cycles and to obtain a deterioration model describing the deterioration process of strength parameters, some researchers carried out a fitting analysis using different types of functions (Guan et al. 2009; Md et al. 2016).

Strength deterioration of compacted loess due to D–W cycles is influenced by the number of D–W cycles n and D–W cycles path (i.e., the upper and lower bounds of the D–W cycles). D–W cycles path can be described as the D–W amplitude A and lower bounds of the D–W cycles w_l (Sumner and Loubser 2010). Besides, dry density ρ controls the pore and permeability characteristics in compacted loess, and thus is another influencing factor that controls strength deterioration of compacted loess (Sitharam 1999; Nowamooz and Masrouri 2010). However, current studies only focus on partially controlling factors, and no comprehensive deterioration model has been presented thus far.

In this study, the influence of the number of D–W cycles n , D–W amplitude A , lower bounds of the D–W cycles w_l , and dry density ρ on the strength deterioration of compacted loess was investigated experimentally. Triaxial tests and environmental scanning electron microscope (ESEM) examinations were carried out to study changes in the strength parameters and the microstructure of the compacted loess during the D–W process. By analyzing the strength parameters through the occurrence of D–W cycles under different influencing factors, a comprehensive compacted loess deterioration model (CLDM) that considers n , A , w_l , and ρ was established. Finally, the CLDM was applied to the finite element method (FEM) using ABAQUS FEM software, and slope stability analysis was carried out while considering D–W cycles.

Experimental process

Sample preparation

The loess in this study was sampled from the Yan'an New-City High Fill Project, which is located in Yan'an city, Shaanxi province, Northwestern China (Fig. 1), in the Q3 loess layer of an excavation area (loess hill and loess ridge). Physical parameters of the loess sample were obtained through soil sample tests and are shown in Table 1. The soil can be classified as a moderate liquid limit clay soil. The gradation curve is shown in Fig. 2, and the nonuniformity and curvature coefficients are $C_u = 25$ and $C_c = 5.44$, respectively, indicating the soil has uneven gradation.

First, the obtained loess samples were crushed and dried to a constant weight at 105 °C and sieved using a 2-mm sieve to discard large particles. Loess samples were humidified up to

an optimal water content and kept in a sealed container for 7 days, to homogeneously distribute water in the sample. Then, the loess samples were placed into a cylindrical steel mold (diameter $\Phi = 39.1$ mm and height $H = 80$ mm) and densely compacted to form triaxial test samples with different dry densities. The dry density of each sample was controlled by calculating the weight and volume of the compacted soil. Finally, the triaxial test samples were kept in a sealed container for 2 days in order to homogeneously distribute water in the sample.

Drying–wetting cycle process

The D–W process consists of humidification and dehumidification processes. Natural water migration in soils due to rainfall infiltration, change in groundwater table, or water evaporation are all approximately one-dimensional. Different water migration direction will lead to different strength deterioration of compacted loess (Tang et al. 2011). In order to accurately simulate the influence of natural D–W cycles on the shear strength of compacted loess, the side surfaces of the triaxial test samples were wrapped in plastic film during the humidification and dehumidification processes. This ensures that water in the triaxial test samples can only migrate through the top and bottom surfaces of the samples, thus approximately simulating one-dimensional water migration. The humidification process is realized by using a burette to add water to the triaxial test samples, while the dehumidification process is completed by drying in an oven at a low temperature. The water content samples during humidification and dehumidification was determined from the gross weight. After the D–W process and before the shear test, samples were kept in a sealed container for 2 days in order to homogeneously distribute water in the sample. The dry density of the triaxial test samples was verified to be unchanged before and after the cyclic D–W by examining the height and circumference of the samples during the process to ensure that no soil mass loss occurred during the cyclic D–W process.

Experiment setup

Dry density in compacted soil is the main factor affecting construction quality. Compared with undisturbed soil, the strength parameters of the compacted soil are highly correlated with dry density (Mei et al. 2016), thus it is of practical significance to study how dry density affects the strength parameters of compacted loess during D–W cycles. Besides, due to uncertainty in environmental factors, D–W cycles in soil structures are not constant at different depths or positions. Therefore, two groups of D–W triaxial tests on compacted loess were considered in this paper:

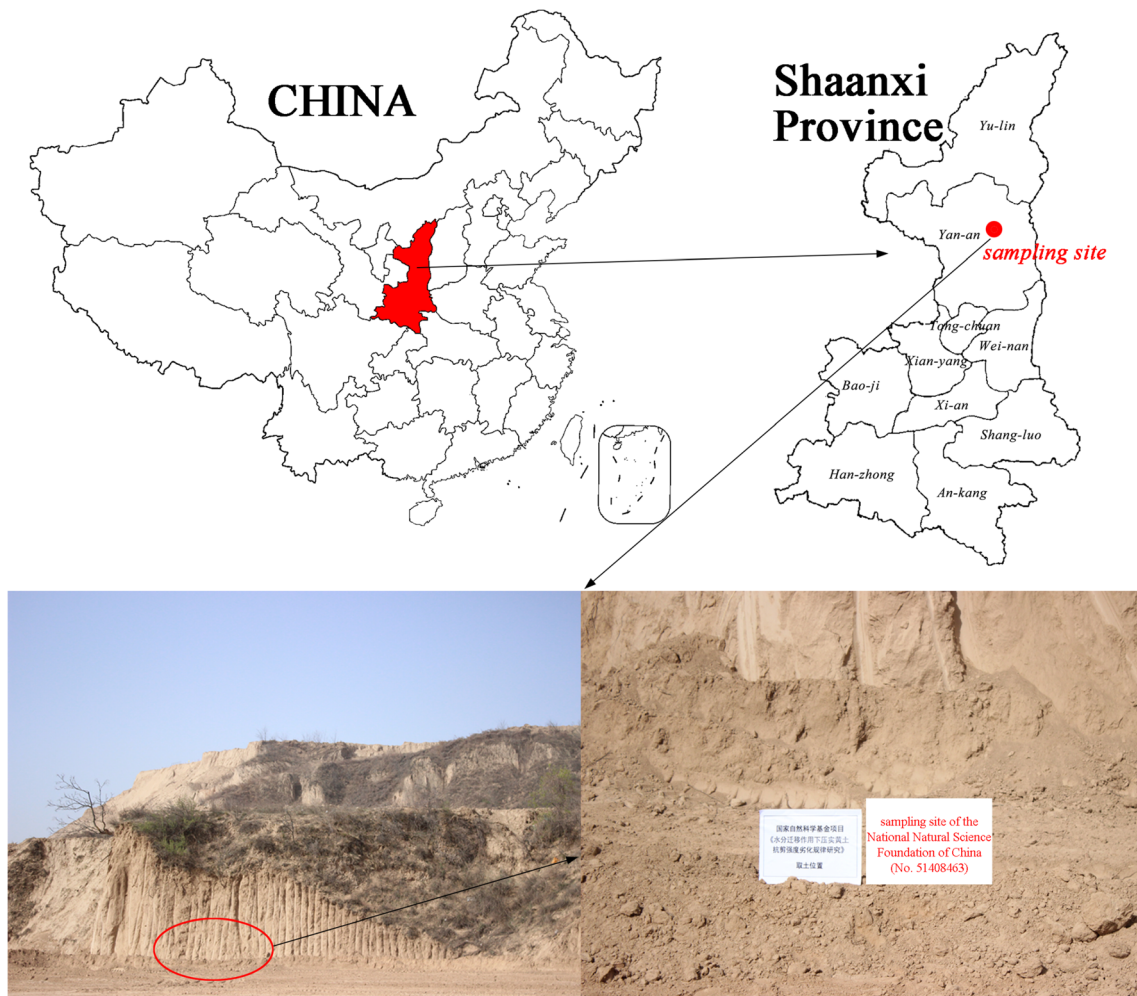


Fig. 1 Sampling location

- 1) **Dry density group:** samples with different ρ values were considered, while A and w_l were held constant. In this part, influence of dry density on the strength deterioration of compacted loess during D–W cycles was studied.
- 2) **D–W cycle path group:** ρ was held constant, while different A and w_l values were considered. In this part, influence of D–W cycle path on the strength deterioration of compacted loess during D–W cycles was studied.

Dry density group

In the dry density group, ρ in the triaxial test samples varied from $\rho = 1.4 \text{ g/cm}^3$ to 1.7 g/cm^3 in 0.1 g/cm^3 , while A and w_l were held constant. w_l was set to 4.5%, which is the average natural water content of the sampled loess, while the upper

bound water content was set to the saturated water content. Twelve D–W cycles were considered, and samples were selected for triaxial tests after 0, 1, 3, 6, 9, and 12 D–W cycles. The serial numbers and corresponding D–W paths are shown in Table 2. We use the notation $\rho - n$ to describe each pair of dry density value and the number of D–W cycles (e.g., 1.4–1 represents samples with dry density of 1.4 g/cm^3 after 1 D–W cycle).

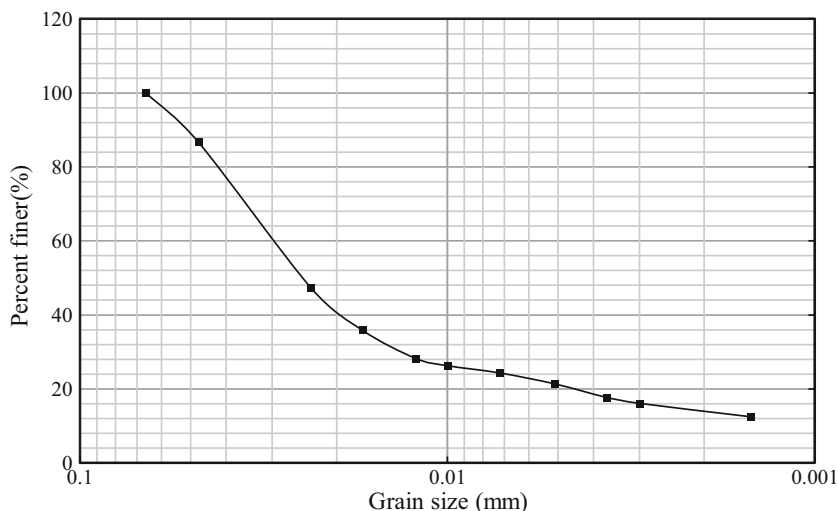
D–W cycle path group

In the D–W cycle path group, ρ was fixed to 1.6 g/cm^3 , which is the average dry density of a completed fill body. Four types of D–W paths were considered in this group, i.e., 4.5%–23.3%, 13.9%–23.3%, 4.5%–13.9%, and 9.2%–18.6%; these are denoted by $\alpha, \beta, \gamma,$ and δ in Table 3, respectively. A values

Table 1 Physical parameters of the loess sample

Liquid limit	Plastic limit	Plastic index	Maximum dry density	Optimal water content
33.42%	19.71%	13.71	1.76 g/cm^3	17.09%

Fig. 2 Grain gradation curve



for series α , β , γ , and δ are 18.8%, 9.4%, 9.4%, and 9.4%, respectively. w_l values for series α , β , γ , and δ are 4.5%, 13.9%, 4.5%, and 9.2%, respectively. By comparing the test results between series α and series β , γ , and δ , the influence of cycle amplitude on the strength deterioration can be analyzed, while by comparing the test results among series β , γ , and δ , the influence of the lower bound of D–W cycles on the strength deterioration can be analyzed.

Triaxial tests

The unsaturated strength of compacted loess samples after D–W cycles was obtained through undrained-unconsolidated (UU) triaxial tests at a water content of 12% (average water content of filling construction). Loading rate of the tests was set as 0.5% strain per minute. The confining pressure σ_3 for each series was set to 100 kPa, 200 kPa, and 300 kPa.

Results and analysis

Dry density group

Stress–strain curves of different numbers of D–W cycles and different ρ value were obtained through UU triaxial

tests, and the results are shown in Fig. 3. The shear stress limit $(\sigma_1 - \sigma_3)_{max}$ for each stress–strain curve was determined from either the peak value (if existed) or from the shear stress when the corresponding axial strain ϵ_1 is 15%.

Shear strength analysis

One can see from the stress–strain curves in Fig. 3 that D–W cycles caused evident strength deterioration in the compacted loess. The stress strain curve decreases gradually as n increases. Decreases in the stress–strain curves tend to be stable. The stress–strain curves changes from strain-hardening to strain-softening as dry density increases, but strain-softening occurs only when the dry density is 1.7 g/cm^3 and the confining pressure is 100 kPa. This is because the sample preparation process is similar to the process of giving soil samples a pre-consolidation pressure. The greater the dry density, the more obvious the effect will be. When the dry density is high and the confining pressure is small, the pre-consolidation effect will be expressed. Moreover, D–W cycles have no influence on the type of stress–strain curves of compacted loess.

Table 2 Dry density group

Serial numbers	D–W path	Serial numbers	D–W path	Serial numbers	D–W path	Serial numbers	D–W path
1.4-0	4.5% 29.2%	1.5-0	4.5% 26.0%	1.6-0	4.5% 23.3%	1.7-0	4.5% 20.5%
1.4-1		1.5-1		1.6-1		1.7-1	
1.4-3		1.5-3		1.6-3		1.7-3	
1.4-6		1.5-6		1.6-6		1.7-6	
1.4-9		1.5-9		1.6-9		1.7-9	
1.4-12		1.5-12		1.6-12		1.7-12	

Table 3 Numbering of the dry density group

Serial numbers	D–W path	Serial numbers	D–W path	Serial numbers	D–W path	Serial numbers	D–W path
α -0	4.5% 23.3%	β -0	13.9% 23.3%	γ -0	4.5% 13.9%	δ -0	9.2% 18.6%
α -1		β -1		γ -1		δ -1	
α -3		β -3		γ -3		δ -3	
α -6		β -6		γ -6		δ -6	
α -9		β -9		γ -9		δ -9	
α -12		β -12		γ -12		δ -12	

Strength analysis

The deterioration curves showing cohesion c and friction angle φ for different ρ values are shown in Figs. 4 and 5, respectively. According to Figs. 4 and 5, c and φ of the compacted loess decrease as n increases, and they tend to become stable when n reaches a certain number. In addition, one can see that the influence of the D–W cycles on c is obviously greater than that of φ . Regularity in the deterioration of c is also stronger, and similar results can be found in the literature (Zeng et al. 2012; Pineda 2014; Md et al. 2016). For a given n value, c and φ of the compacted loess increases as ρ increases, as shown in Figs. 6 and 7. This increase pattern is the same for different n values, indicating that D–W cycles had little influence on the relationship between ρ and the strength parameters.

Deterioration rate

In order to quantitatively study the trend in the deterioration of c and φ caused by D–W cycles, the deterioration rate (DR) of the strength parameters was introduced and is defined by Eq. (1):

$$DR_{c(\varphi)} = \frac{V_i - V_a}{V_i} \times 100\% \tag{1}$$

where V_i is the initial value of c and φ , while V_a is the value of c and φ after D–W cycles. According to Eq. (1), the deterioration rates of c and φ were calculated based on the strength parameter results and are shown in Figs. 8, 9, and 10. The functional relationship between deterioration rates of c and φ with the number of D–W cycles (DR - n) was determined by fitting the data to a hyperbolic function as defined in Eq. (2):

$$DR_{c(\varphi)} = a_{c(\varphi)} \frac{a_{c(\varphi)}}{1 + \frac{a_{c(\varphi)}}{b_{c(\varphi)}} n} \tag{2}$$

where $DR_{c(\varphi)}$ is the deterioration rate of cohesion or friction angle, $a_{c(\varphi)}$ is the maximal deterioration rate obtained from the test results, n is the number of D–W cycles, and $b_{c(\varphi)}$ is the fitting parameter that controls the development of the deterioration rate. A bigger $b_{c(\varphi)}$ denotes a lower development speed

of the deterioration rate.

A hyperbolic function is capable of representing the convergence trend of the deterioration process and only consists of two fitting parameters that have clear physical meaning and thus was chosen to be the fitting function in this paper. The fitting curve and fitting parameters are shown in Figs. 8, 9, and 10 and Table 4.

One can see from Table 4 and Figs. 8 and 9 that the correlation indices (R^2) are all greater than 0.9, indicating that Eq. (2) appropriately models deterioration. Figure 10 shows the relationship between ρ and the fitting parameters a_c , b_c . One can see that ρ has a significant influence on the maximum deterioration rate and the development speed of cohesion deterioration, and the relationship can be described by an exponential function (also shown in Fig. 10). The maximal deterioration rate of cohesion a_c decreases from 88.34% to 36.01% as ρ increases, indicating that loess compaction can help to reduce the deterioration effect of D–W cycles on c . In addition, b_c increases as ρ increases. According to the definition of b_c , the critical value of n at which deterioration saturates will be larger as ρ increases, indicating that increasing ρ helps to suppress deterioration due to D–W cycles. On the contrary, the fitting parameters of φ , a_φ , and b_φ show minor changes at larger ρ values, so a_φ and b_φ can be considered independent of ρ . The average values of the a_φ and b_φ are 13.96% and 1.99, respectively. Table 5 shows a summary of the fitting results.

Deterioration mechanism analysis

A Quanta 200 environmental scanning electron microscope (ESEM) was used to study changes in the microstructure of compacted loess before and after several D–W cycles. Figure 11 shows a comparison of the microstructure of compacted loess for different dry density values before and after 12 D–W cycles. It can be seen that multiple D–W cycles can promote changes in particle type and in the contact type between particles. After 12 D–W cycles, the number of angular particles and face contacts between particles decreased, while more round particles and point contacts emerged. In addition, the degree of fragmentation, degree of particle aggregation, and pore structures between particles increased

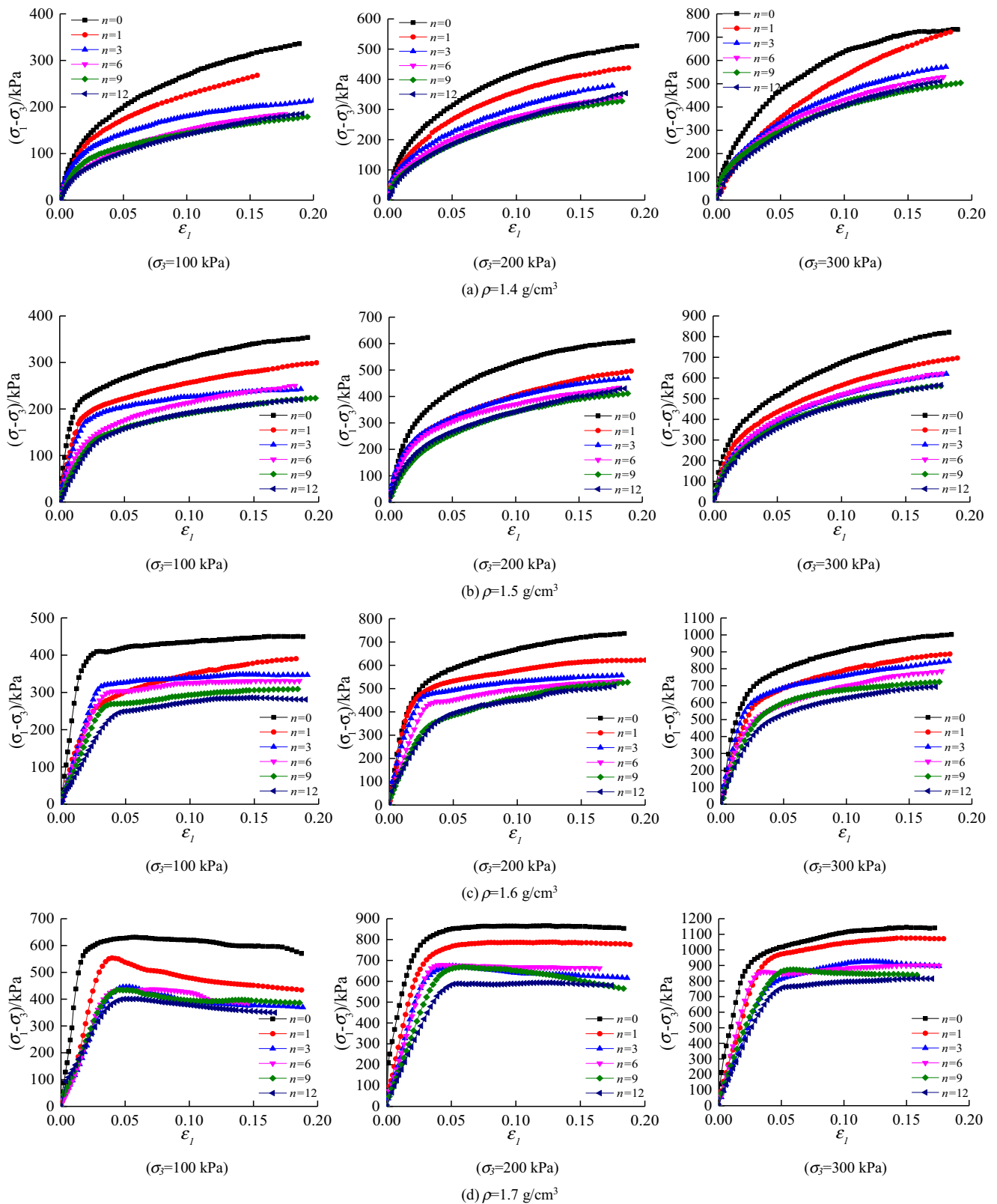


Fig. 3 Stress–strain curves of the dry density group

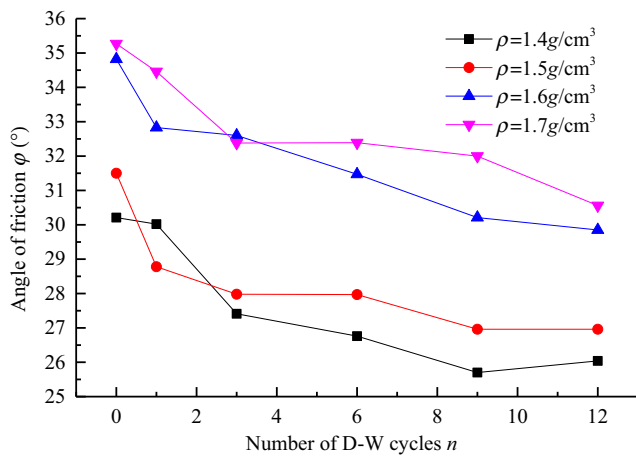


Fig. 4 Deterioration of φ at different dry density values

(Pires et al. 2008). A combination of the above effects results in the deterioration of the strength of compacted loess.

One can also see from Fig. 11 that the pores between the compacted loess particles gradually decrease as dry density increases. This leads to closer contact and stronger interlocking between loess particles, thus leading to larger c and φ values. The cohesive strength of compacted loess is composed of its original cohesion and adsorption strength. The original cohesion is stable, while the adsorption strength is determined by matrix suction and capillary pressure.

The D–W cycles led to an increase in the amount of pores, which resulted in a smaller matrix suction and capillary pressure. This leads to a decrease in the cohesive strength of compacted loess. Regarding friction strength deterioration, the decrease in the friction and interlocking effect is primarily caused by abrasion and fragmentation of the particles. By

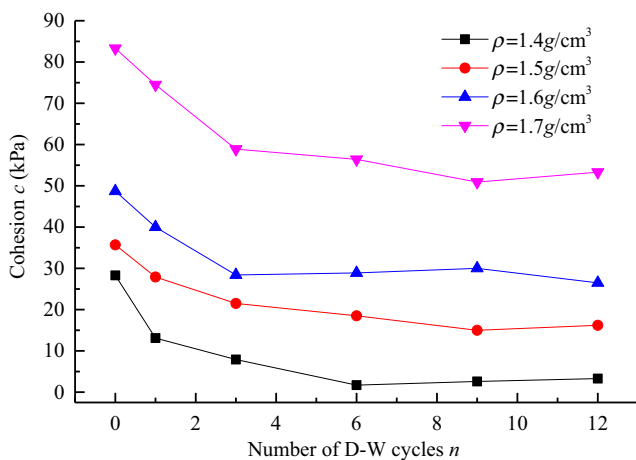


Fig. 5 Deterioration of c at different dry density values

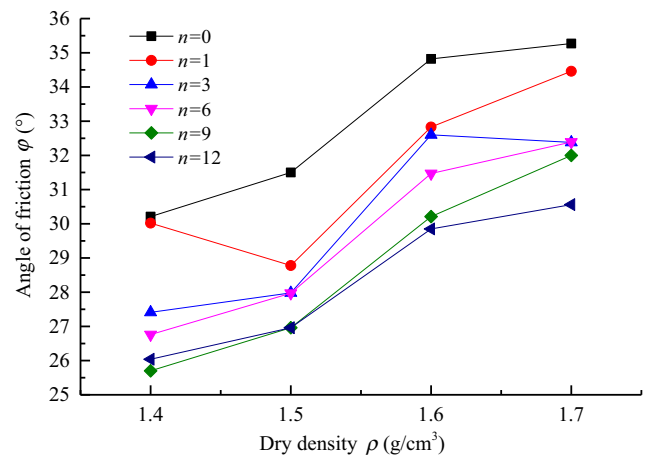


Fig. 6 Influence of dry density on φ

comparing the microstructure images of different dry densities, it can be seen that when the dry density was increased, increase of the pores, abrasion and fragmentation of the particles, and the change in contact type between the particles are restrained. This is because the non-uniformity of the pores in compacted loess leads to non-uniform changes in the matrix during the D–W cycles; this is one of the main causes of shear strength deterioration (Wang and Li 2015; Wang et al. 2016a, b). An increase in dry density helps to reduce this non-uniformity. Therefore, increasing dry density will lead to a smaller maximal deterioration rate and lower the deterioration speed of the cohesion c of compacted loess. Furthermore, the abrasion and fragmentation of the particles are mainly affected by the flux of water content variation. Therefore, an increase in dry density has no observable effect on the deterioration of friction angle.

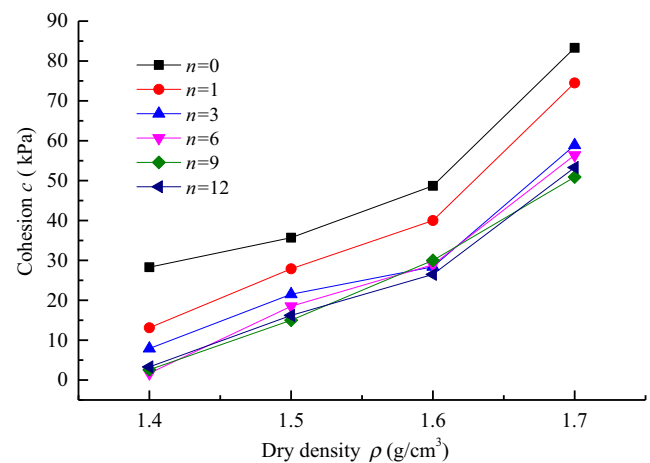


Fig. 7 Influence of dry density on c

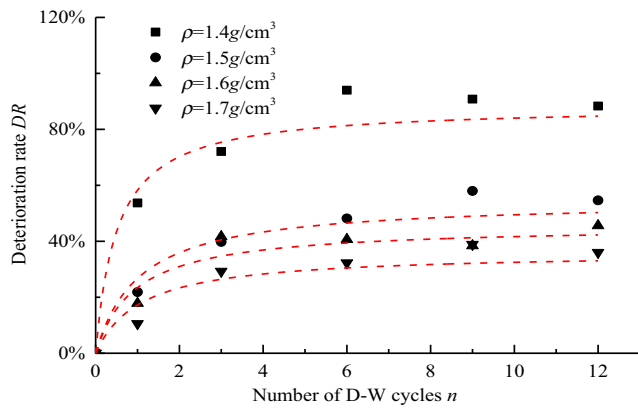


Fig. 8 Deterioration rate and fitting curve for c at different dry density values

D–W cycle path group

Strength deterioration analysis

The stress–strain curves for the D–W cycle path group ($n = 1, 6, \text{ and } 12$ were chosen to show the pattern) are shown in Fig. 12 for comparison. In this group, the D–W cycle paths of series $\alpha, \beta, \gamma,$ and δ are 4.5%–23.3% (lower bound – upper bound), 13.9%–23.3%, 4.5%–13.9%, and 9.2%–18.6%, respectively. The D–W cycle amplitude A for series α is 18.8%, and $A = 9.4\%$ for series $\beta, \gamma,$ and δ , and the lower bounds of the D–W cycle w_l is 13.9%, 4.5%, and 9.2%, respectively. One can see from Fig. 12 that the stress–strain curve for series α is clearly lower than that for series $\beta, \gamma,$ and δ . As for series $\beta, \gamma,$ and δ , the stress–strain curves are close to each other, indicating that the D–W cycle amplitude A has a more significant effect on strength deterioration in compacted loess.

The strength parameters of compacted loess are shown in Figs. 13 and 14. One can see that c and φ both decrease as n increases. It is clear that strength deterioration for series α is the largest, indicating that A has a more significant effect on

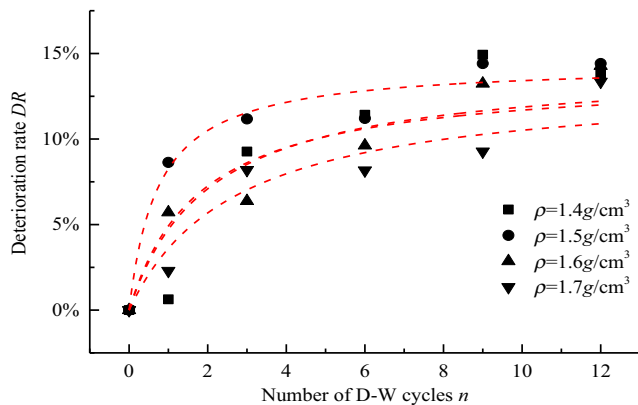


Fig. 9 Deterioration rate and fitting curve for φ at different dry density values

strength deterioration. For c , deterioration of the three series in descending order are: γ, δ, β , indicating that w_l has a significant influence on deterioration of c , and a smaller w_l leads to a greater deterioration of c . For φ , deterioration for series $\beta, \gamma,$ and δ shows no clear difference, indicating that w_l has negligible influence on deterioration of φ .

The strength parameter data was converted to a deterioration rate (DR) using Eq. (1), and the relationship between DR and n is fit to Eq. (2). The fitting results are shown in Table 6 and Figs. 15 and 16. The relationship between $a_c, b_c, a_\varphi, b_\varphi,$ and A and w_l is analyzed by curve fitting, and the results are shown in Figs. 17, 18, 19, and 20.

1) Maximal deterioration rate a_c, a_φ

One can see from Fig. 17 that a_c decreases linearly as w_l increases, while a_φ has no clear dependence on w_l . The value of a_φ can be set as the average value of series $\beta, \gamma,$ and δ , i.e., $a_\varphi = 7.0\%$ when $A = 9.4\%$. Figure 18 shows the relationship between $a_c, a_\varphi,$ and A . It should be mentioned that point (0,0) in Fig. 18 is also treated as a data point in the fitting analysis because the deterioration rate is clearly 0% when A is 0%, i.e., the compacted loess is not affected by D–W cycles. One can see from Fig. 18 that a_c and a_φ both linearly increase as A increases, while a_c increases faster than a_φ .

2) Development speed parameters b_c, b_φ

Table 6 shows that the b_φ values for series $\beta, \gamma,$ and δ are 1.58696, 0.58063, and 1.62923, respectively. The results for series β and δ are similar, but the results for series γ are very different. Considering the fact that the fitting index φ for series γ is 0.73 and data dispersion is too large (as shown in Fig. 16), data from series γ was ignored, and b_φ was set as the average value of series β and δ , i.e., $b_\varphi = 1.6081$ when $A = 9.4\%$. Moreover, b_c can be regarded as a linear function of w_l , as shown in Fig. 19. Furthermore, the relationship between $b_c, b_\varphi,$ and A is also linear, as shown in Fig. 20.

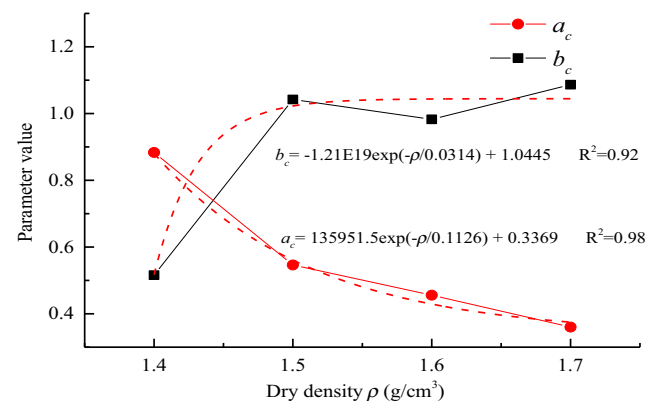


Fig. 10 Relationship between dry density and coefficient a_c and b_c

Table 4 Fitting parameters for different c , φ values at different dry densities

D–W cycles (n)	Dry density ρ (g/cm ³)							
	1.4		1.5		1.6		1.7	
	c (kPa)	φ (°)	c (kPa)	φ (°)	c (kPa)	φ (°)	c (kPa)	φ (°)
a	88.34%	13.80%	54.62%	14.41%	45.59%	14.27%	36.01%	13.35%
b	0.51579	1.807	1.04214	1.7459	0.94271	2.0244	1.08659	2.399
R^2	0.96	0.84	0.95	0.97	0.94	0.91	0.91	0.91

In summary, a_c and a_φ increase linearly as A increases, and the development speed of the deterioration rate of c and φ decreases linearly as A increases when w_l is held constant. a_c decreases linearly as w_l increases, and the development speed of the deterioration rate of c decreases as w_l increases when A is held constant. a_φ and the development speed of the deterioration rate of φ are not influenced by w_l . These results are summarized in Table 7.

Deterioration mechanism analysis

As mentioned in Section 3.1.4, decreased adsorption strength is the main cause of cohesion deterioration, which is closely related to the pore characteristics of soil. From a microscopic perspective, the matric suction in soil is caused by the surface tension on the liquid bridge between particles. During the dehumidification process, the volume of the liquid bridge decreases, and the matric suction increases

Table 5 Parameter fitting results

Fitting parameters			
Cohesion c		Friction angle φ	
a_c	b_c	a_φ	b_φ
$a_c = 135,951.5 \exp(-\rho/0.1126) + 0.3369$	$b_c = -1.21E19 \exp(-\rho/0.0314) + 1.0445$	13.96%	1.99

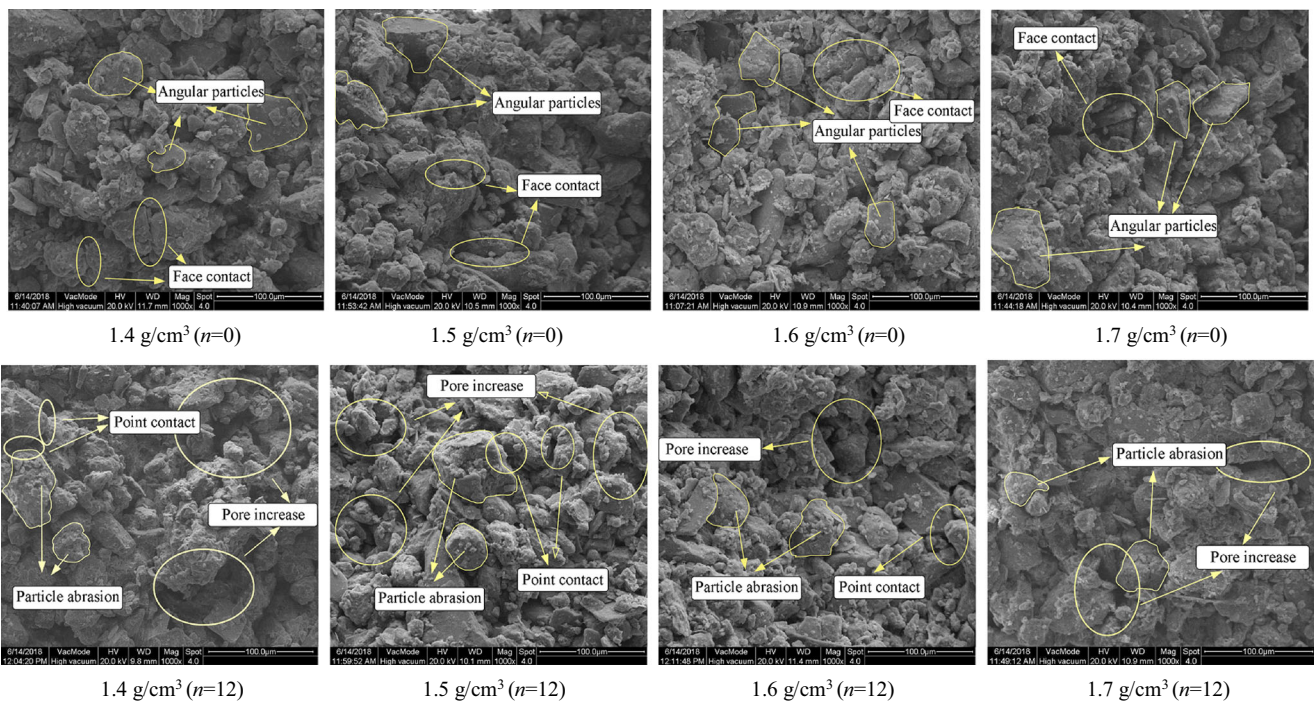


Fig. 11 ESEM microstructure of compacted loess

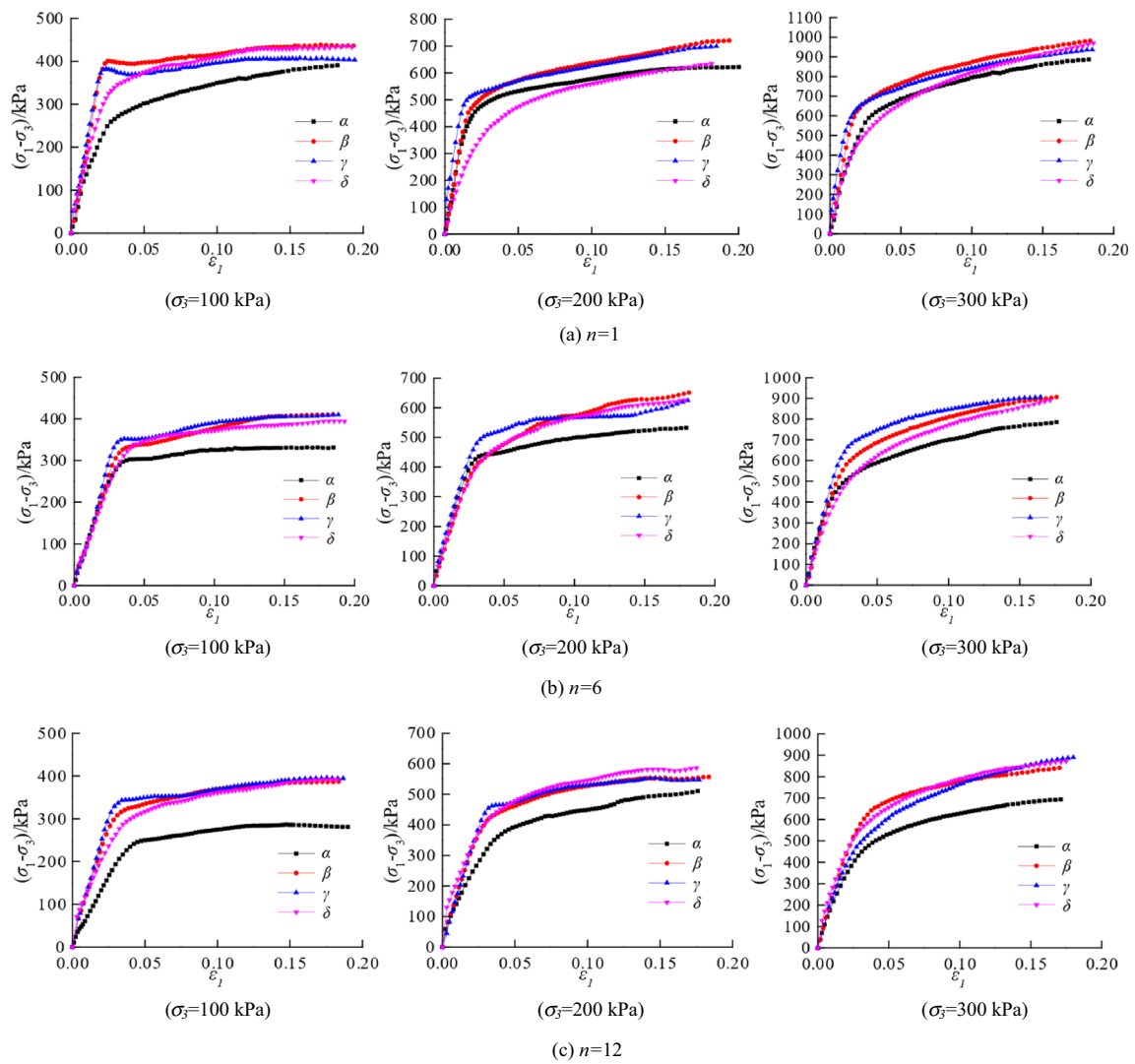


Fig. 12 Stress–strain curves of D–W path group

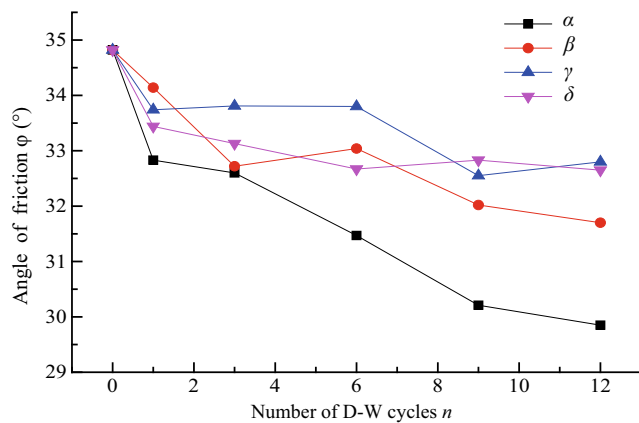


Fig. 13 Deterioration of φ for different D–W paths

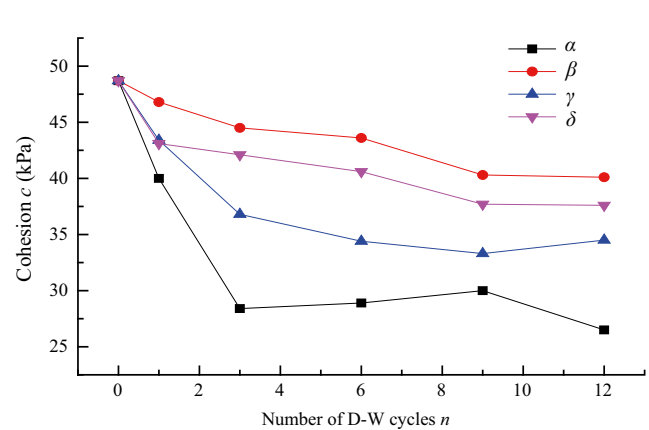


Fig. 14 Deterioration of c for different D–W paths

Table 6 Fitting parameters for different c , φ values under different D–W paths

D–M cycles (n)	Serial numbers					
	β		γ		δ	
	c (kPa)	φ (°)	c (kPa)	φ (°)	c (kPa)	φ (°)
a	17.66%	8.96%	29.16%	5.80%	22.79%	6.23%
b	0.84778	1.58696	1.26831	0.58063	2.4248	1.62923
R^2	0.90	0.90	0.91	0.73	0.93	0.98

gradually (Soulié et al. 2010). When the matric suction reaches a critical value, the liquid bridge between the soil particles breaks down, which leads to soil cracking (Wang et al. 2016a, b). On the one hand, increase in D–W cycle amplitude A prolongs this cracking process, resulting in higher cohesion deterioration. On the other hand, lower water content indicates higher matrix suction and a higher possibility for the breaking down of liquid bridges; this explains why the lower bounds of the D–W cycles' w_l have an observable influence on cohesion deterioration. Regarding friction angle, abrasion and fragmentation of the particles control its deterioration, which is mainly affected by the flux of water content variation. Therefore, A has an observable influence on friction angle deterioration.

Compacted loess deterioration model (CLDM)

The influence of D–W cycles on compacted loess is affected by n , ρ , A , and w_l , and these factors are not constant naturally. Therefore, it is necessary and appropriate to consider the strength deterioration of compacted loess as a function of these factors. According to the results in Section 0, the

cohesion deterioration rate DR_c is a function of n , ρ , A , and w_l ; i.e., $DR_c = f(n, \rho, A, w_l)$. The cohesion deterioration rate DR_φ is a function of n and A ; i.e., $DR_\varphi = g(n, A)$.

Deterioration model of the cohesion of compacted loess

The cohesion deterioration model for compacted loess was obtained through function iteration using the results in Section 0 (Tables 5 and 7):

When $\rho = 1.6 \text{ g/cm}^3$ and $w_l = 4.5\%$, a_c and b_c can be expressed as follows:

$$a_c = 2.56043 \times A b_c = 4.653A + 1.149 \tag{3}$$

The variation in w_l is then taken into consideration:

$$\begin{aligned} a_c &= 2.560 \times A \times \frac{-1.223 \times w_l + 0.345}{-1.223 \times 0.045 + 0.345} \\ &= 8.843 \times A \times \frac{(-1.223 \times w_l + 0.345)}{16.78w_l - 0.030} \\ b_c(4.653A + 1.149) &\times \frac{16.78 \times 0.045 - 0.030}{16.78 \times 0.045 - 0.030} \\ &= 1.379 \times (4.653A + 1.149) \times (16.78w_l - 0.030) \end{aligned} \tag{4}$$

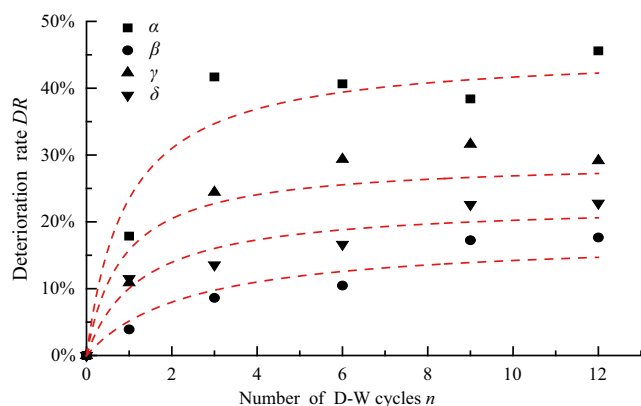


Fig. 15 Deterioration rate and fitting curve for c under different D–W paths

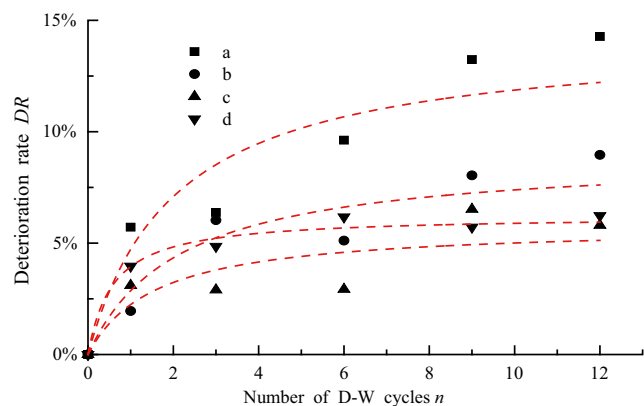


Fig. 16 Deterioration rate and fitting curve for φ under different D–W paths

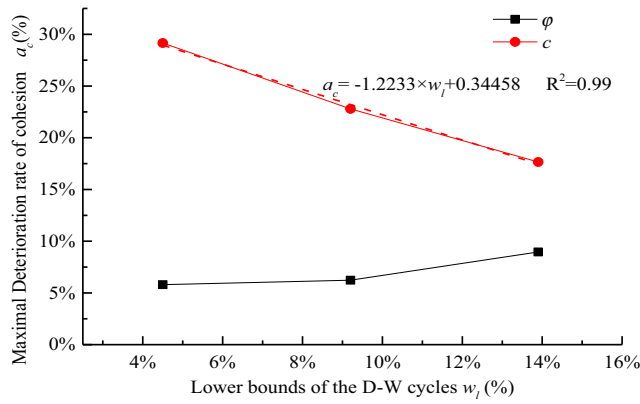


Fig. 17 Relationship between w_l and a_c, a_φ

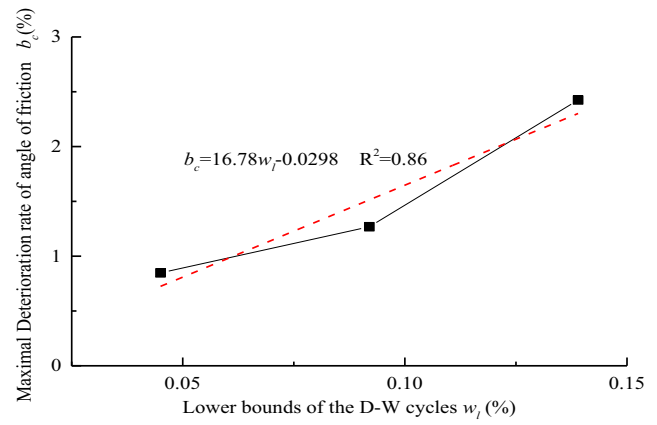


Fig. 19 Relationship between w_l and b_c

Finally, the variation in ρ is considered:

$$\begin{aligned}
 a_c(\rho, A, w_l) &= 8.843 \times A \times (-1.223 \times w_l + 0.345) \\
 &\times \frac{135951 \times \exp(-\rho/0.113) + 0.337}{135951 \times \exp(-1.6/0.113) + 0.337} \\
 &= 20.634 \times A \times (-1.223 \times w_l + 0.345) \\
 &\times (135951.5 \times \exp(-\rho/0.113) + 0.337) \\
 b_c(\rho, A, w_l) &= 1.379 \times (4.653 + 1.149) \\
 &\times \frac{-1.21E19 \times \exp(-\rho/0.113) + 1.0445}{-1.21E19 \times \exp(-1.6/0.0314) + 1.0445} \\
 &= 1.321 \times (4.653A + 1.149) \times (16.78w_l - 0.030) \\
 &\times (-1.21E19 \times \exp(-\rho/0.113) + 1.045)
 \end{aligned} \tag{5}$$

$$DR_c(n, \rho, A, w_l) = a_c(\rho, A, w_l) - \frac{a_c(\rho, A, w_l)}{1 + \frac{n}{b_c(\rho, A, w_l)}} \tag{6}$$

Equations (5) and (6) are the deterioration model for cohesion in compacted loess in this study.

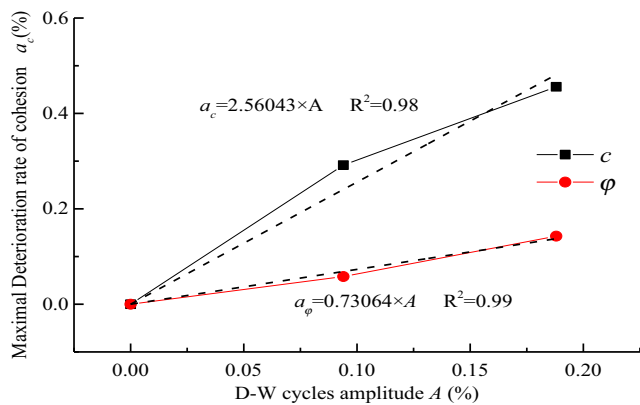


Fig. 18 Relationship between A and a_c, a_φ

Deterioration model for the friction angle in compacted loess

Similarly, combining Eqs. (7) and (8) yields a deterioration model of the friction angle for compacted loess:

$$\begin{aligned}
 a_\varphi(A) &= 0.73064 \times A \\
 b_\varphi(A) &= 1.435A + 0.713
 \end{aligned} \tag{7}$$

$$DR_\varphi(n, A) = a_\varphi(A) - \frac{a_\varphi(A)}{1 + \frac{n}{b_\varphi(A)}} \tag{8}$$

D-W cycle slope stability analysis

Finite element model

On the basis of strength parameter tests on undisturbed soil sampled from a slope, Deng et al. (2017) studied the variation in the factor of safety (FS) of a slope with respect to D-

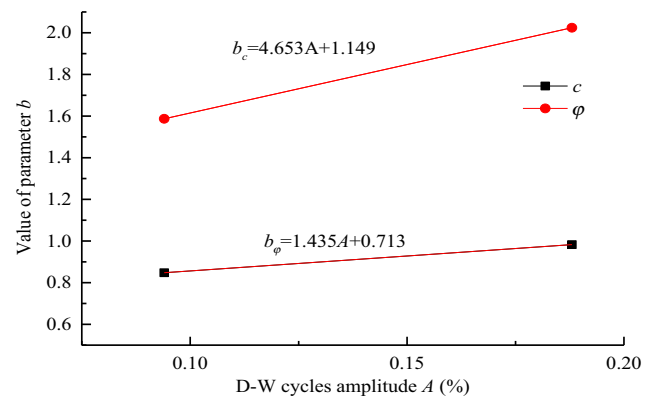


Fig. 20 Relationship between A and b_c, b_φ

Table 7 Parameter fitting results

Variable	Fitting parameters			
	c		φ	
	a_c	b_c	a_φ	b_φ
A (w_l was fixed at 4.5%)	$a_c = 2.56043 \times A$	$b_c = 4.653A + 1.149$	$a_\varphi = 0.73064 \times A$	$b_\varphi = 1.435A + 0.713$
w_l (A was fixed at 9.4%)	$a_c = -1.2233 \times w_l + 0.34458$	$b_c = 16.78w_l - 0.0298$	7.0%	1.6081

W cycles by assigning strength parameters influenced by D–W cycles to slope soil layers. Zeng et al. (2012) studied the influence of D–W cycles on the stability of slopes using the Sweden slice method. However, because environmental factors influence slope soils differently in different locations on the slope, the effect of D–W cycles is also different. For example, soils on the slope surface suffer from stronger D–W cycles caused by rainfall, while deep soils suffer weaker effects from D–W cycles. By incorporating the CLDM obtained in this paper with the FEM, slope stability analysis considering D–W cycle effects was realized. This analysis proceeds as follows:

First, the maximum and minimum values of water content in each element of the slope model after rainfall are obtained through a 2-D slope rainfall infiltration simulation using finite element analysis. The maximum and minimum water contents in each element are used as the upper and lower bounds in D–W cycles, and the deterioration function for soil strength in each element can be obtained from Eqs. (5)–(8). Through a secondary development of finite element software ABAUQS, the strength parameters calculated from the strength deterioration function are independently assigned to each element of the model for a given n value, and the FS of the slope at each n

is calculated using the finite element strength reduction method (SSR).

A typical fill slope from the Yan’an New-City High Fill Project was chosen to establish the finite element model. The slope height is $H = 20$ m, and the slope rate is 1:1.7. The model dimensions are shown in Fig. 21. The slope is composed of homogeneous Q_3 compacted loess. The physical and mechanical parameters of the loess are shown in Table 8, and the soil water characteristic curve (SWCC) obtained from a pressure plate extractor test is shown in Fig. 23. Rainfall was applied to the surface of the slope model. The left boundary is set as a potential seepage boundary, and the remaining boundaries are set as impermeable boundaries (as shown in Fig. 22).

The maximum daily rainfall was set as 139.9 mm/d. Therefore, the rainfall load of in this study was set to 139.9 mm/d, and the rainfall amplitude curve is shown in Fig. 24.

Simulation results

Figure 25 shows the simulation results of water content in the slope model after 0 h, 24 h, 48 h, and 72 h. Figure 26 shows the water content variation curve at 6 locations with different depths under the slope shoulder point. One can see that the variation in water content decreases as buried depth increases, indicating that the influence of D–W cycles caused by rainfall decreases with increased depth of soil. Figure 27 shows the relationship between FS and n . One can see that the FS gradually decreases as n increases, and the variation tends to be stable. The variation in FS is similar to that found for the strength

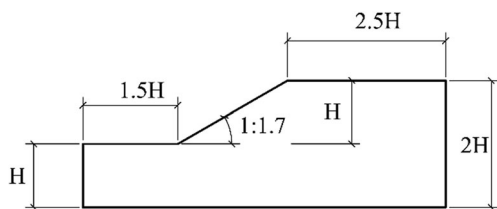
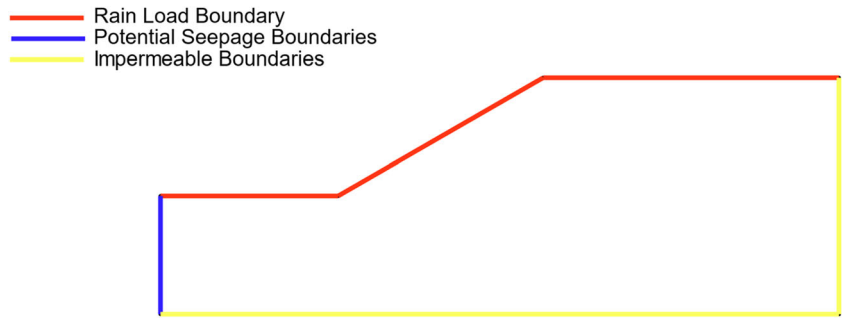


Fig. 21 Model dimensions

Table 8 Physical and mechanical parameters of slope soil

Dry density (g/cm^3)	Permeability coefficient (m/d)	Initial cohesion (kPa)	Friction angle ($^\circ$)
1.6	0.0317	48.7	31.6

Fig. 22 Seepage boundaries



parameters. Furthermore, FS is not significantly affected by rainfall because deeper soils experience lower rainfall infiltration, and the final FS reduction rate is about 17%.

Conclusion

- D–W cycles will deteriorate the shear strength of compacted loess, but there is no obvious effect on the type of stress–strain curve. As the number of D–W cycles increases, the strength gradually decreases and eventually stabilizes at a certain value. Increased dry density ρ will reduce the porosity in the compacted loess and suppresses deterioration. When the dry density increases from 1.4 g/cm³ to 1.7 g/cm³, the maximum cohesion deterioration rate decreases from 88.34% to 36.01%, and the deterioration speed decreases. An increased dry density has no significant effect on friction angle deterioration.

- The maximum cohesion and friction angle deterioration rate linearly increases as the amplitude of the D–W cycles increases, and the development speed of the deterioration rate decreases linearly. When the D–W cycle amplitude is held constant, increasing the lower bounds of the D–W cycle w_l leads to a linear decrease in the maximum deterioration rate and development speed of cohesion deterioration, but it has little influence on the deterioration of the friction angle.
- Cohesion deterioration in compacted loess is a function of the number of D–W cycles, dry density, D–W cycle amplitude, and lower bounds of the D–W cycles. The deterioration in friction angle φ is only a function of D–W cycles and the D–W cycle amplitude. According to fitting analysis of D–W cycle strength test results, a comprehensive compacted loess deterioration model (CLDM) was established and used to analyze the stability of a compacted loess slope by secondary development of finite element software ABAQUS. For the chosen fill slope, the factor of safety is not significantly affected because rainfall infiltration is suppressed in deeper soils.

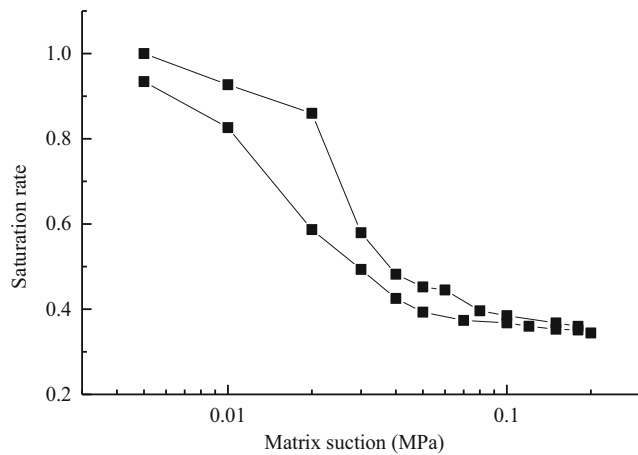


Fig. 23 Soil and water characteristic curve

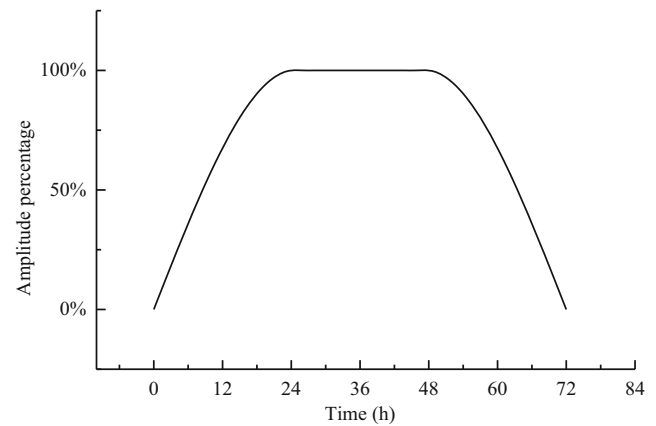
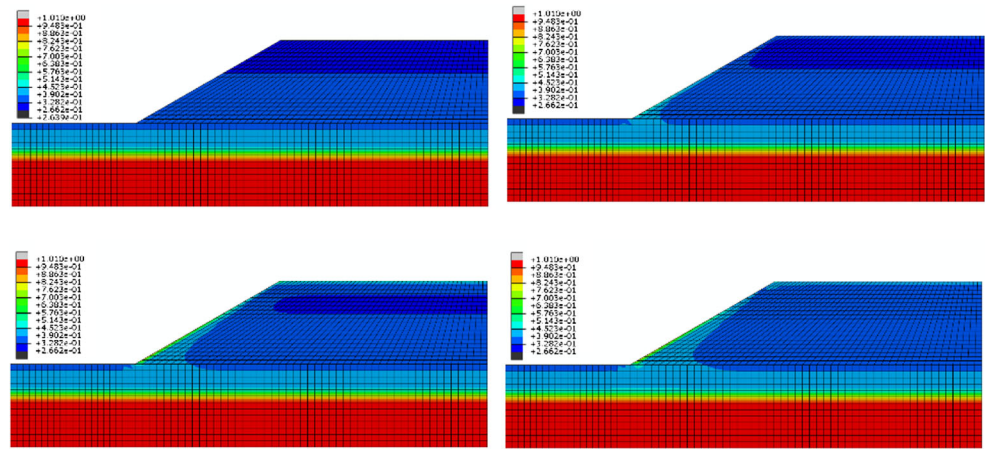


Fig. 24 Rainfall intensity amplitude curve

Fig. 25 Water content field calculation results



(0 h, 24 h, 48 h, 72 h, successively)

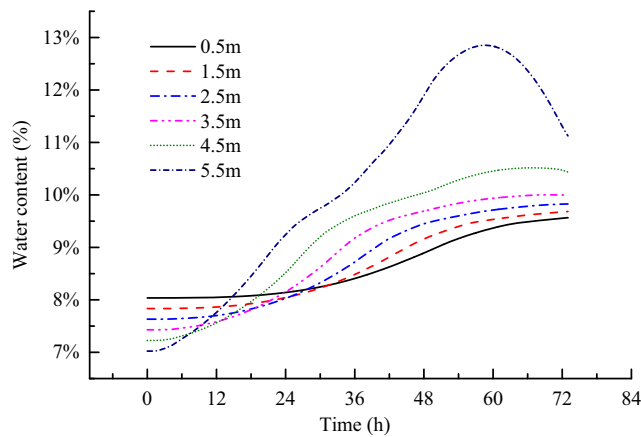


Fig. 26 Water content change curve at different points under slope shoulder of the model

- This study also has certain limitations. For example, only the unsaturated strength of compacted loess at a water content of 12% was analyzed. However, D–W cycles may also influence the mechanical behavior of compacted loess for different water content. The dry density in the soils on a slope is not constant and can be described as a random field, and a random finite element model should be constructed to obtain a more reliable stability analysis. Therefore, further studies are required to improve on these results.

Acknowledgements This work was supported by the National Natural Science Foundation of China (no. 51408463), and the Special Research Project of Shaanxi Provincial Education Department (grant no. 17JK0424).

References

Aldood A, Bouasker M, Al-Mukhtar M (2014) Impact of wetting–drying cycles on the microstructure and mechanical properties of lime-stabilized gypseous soils. *Eng Geol* 174:11–21

Allam MM, Sridharan A (1981) EFFECT OF WETTING AND DRYING ON SHEAR STRENGTH. *J Geotech Eng Div* 107(4): 421–438

Al-Obaydi MA, Al-Kiki IM, Al-Zubaydi AH (2010) Strength and durability of gypseous soil treated with waste lime and cement. *Al Rafdain Eng J* 18(1):28–42

Al-Zubaydi A (2011) Effect of static soaking under different temperatures on the lime stabilized gypseous soil. *Tikrit J Eng Sci* 18(3):42–51

Benatti J, Miguel MG, Rodrigues RA, Vilar O M (2011) Collapsibility study for tropical soil profile using oedometric tests with controlled suction. *Unsaturated soils* (Eds E. Alonso and a. gens) 1:193–198

Chen R, Ng CWW (2013) Impact of wetting–drying cycles on hydro-mechanical behavior of an unsaturated compacted clay. *Appl Clay Sci* 86:38–46

Clarke D, Smethurst JA (2010) Effects of climate change on cycles of wetting and drying in engineered clay slopes in England. *Q J Eng Geol Hydrogeol* 43(4):473–486

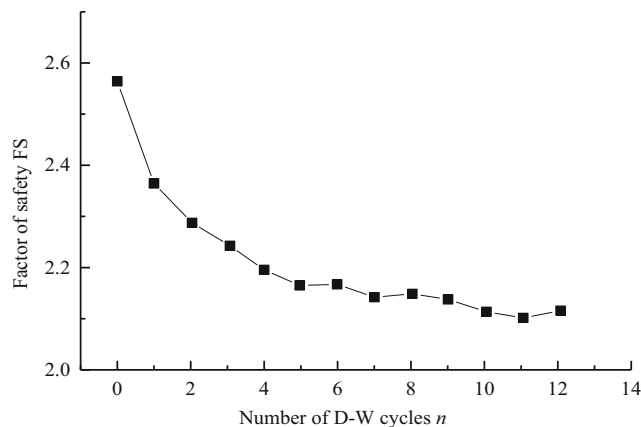


Fig. 27 Variation in FS with the frequency of D–W cycles

- Estabragh AR, Moghadas M, Javadi AA (2013) Effect of different types of wetting fluids on the behaviour of expansive soil during wetting and drying. *Soils Found* 53(5):617–627
- Guan GS, Rahardjo H, Choon LE (2009) Shear strength equations for unsaturated soil under drying and wetting. *J Geotech Geoenviron* 136(4):594–606
- Kampala A, Horpibulsuk S, Prongmanee N, Chinkulkijniwat A (2013) Influence of wet-dry cycles on compressive strength of calcium carbide residue – Fly ash stabilized clay. *J Mater Civ Eng* 26(4):633–643
- Kholghifard M, Ahmad K, Ali N, Kassim A, Kalatehjari R (2014) Collapse/swell potential of residual laterite soil due to wetting and drying-wetting cycles. *Natl Acad Sci Lett* 37(2):147–153
- Li GY, Wang F, Ma W, Fortier R, Mu Y, Mao Y, Hou X (2018) Variations in strength and deformation of compacted loess exposed to wetting-drying and freeze-thaw cycles. *Cold Reg Sci Technol* 151:159–167
- Md SH, Ling-Wei K, Song Y (2016) Effect of drying-wetting cycles on saturated shear strength of undisturbed residual soils. *Am J Civil Eng* 4(4):143–150
- Mei Y, Hu CM, Yuan YL, Wang XY, Zhao N (2016) Experimental study on deformation and strength property of compacted loess. *Geomech Eng* 11(1):161–175
- Nowamooz H, Masroufi F (2010) Influence of suction cycles on the soil fabric of compacted swelling soil. *Compt Rendus Geosci* 342(12):901–910
- Pineda JAREDG (2014) Shear strength degradation in claystones due to environmental effects. *Géotechnique* 64(6):493–501
- Pires LF, Bacchi OOS, Reichardt K (2005) Gamma ray computed tomography to evaluate wetting/drying soil structure changes. *Nucl Instrum Methods Phys Res, Sect B* 229(3):443–456
- Pires LF, Cooper M, Cássaro FAM, Reichardt K, Bacchi OOS, Dias NMP (2008) Micromorphological analysis to characterize structure modifications of soil samples submitted to wetting and drying cycles. *Catena* 72(2):297–304
- Rao SM, Revanasiddappa K (2006) Influence of cyclic wetting drying on collapse behaviour of compacted residual soil. *Geotech Geol Eng* 24(3):725–734
- Rayhani MHT, Yanful EK, Fakher A (2008) Physical modeling of desiccation cracking in plastic soils. *Eng Geol* 97(1–2):25–31
- Rayhani MH, Yanful EK, Fakher A (2007) Desiccation-induced cracking and its effect on the hydraulic conductivity of clayey soils from Iran. *Can Geotech J* 44(3):276–283
- Roshani A, Fall M, Kennedy K (2018) Microstructural, hydraulic conductivity and geochemical changes of drying mature fine oil sand tailings in column experiments. *Int J Min Reclam Environ* 32(4):239–253
- Sitharam TG (1999) Micromechanical modeling of granular materials: effect of confining pressure on mechanical behavior. *Mech Mater* 31(10):653–665
- Soulié F, Cherblanc F, Youssoufi MSE, Saix C (2010) Influence of liquid bridges on the mechanical behaviour of polydisperse granular materials. *Int J Num Anal Methods Geomech* 30(3):213–228
- Sumner PD, Loubser MJ (2010) Experimental sandstone weathering using different wetting and drying moisture amplitudes. *Earth Surf Process Landforms* 33(6):985–990
- Tang CS, Cui YJ, Shi B, Tang AM, Liu C (2011) Desiccation and cracking behaviour of clay layer from slurry state under wetting–drying cycles. *Geoderma* 166(1):111–118
- Taylor SR, McLennan SM, McCulloch MT (1983) Geochemistry of loess, continental crustal composition and crustal model ages. *Geochim Cosmochim Acta* 47(11):1897–1905
- Wang D, Tang C, Cui Y, Shi B, Li J (2016a) Effects of wetting–drying cycles on soil strength profile of a silty clay in micro-penetrometer tests. *Eng Geol* 206:60–70
- Wang X, Li J (2015) A novel liquid bridge model for estimating SWCC and permeability of granular material. *Powder Technol* 275:121–130
- Wu J, Yuan J, Ng CWW (2012) Theoretical and experimental study of initial cracking mechanism of an expansive soil due to moisture-change. *J Cent South Univ* 19(5):1437–1446
- Zeng ZT, Lu HB, Zhao YL (2012) Wetting-drying effect of expansive soils and its influence on slope stability. *Appl Mech Mater* 170-173:889–893
- Deng HF, Xiao Y, Fang JC, Zhang HB, Wang CXJ, Cao Y (2017) Shear strength degradation and slope stability of soils at hydro-fluctuation belt of river bank slope during drying-wetting cycle. *Rock Soil Mech* 38(9):2629–2638 in Chinese
- Wang F, Li GY, Mu YH, Zhang P, Wu YH, Fan SZ (2016b) Experimental study of deformation characteristics of compacted loess subjected to drying-wetting cycle. *Rock Soil Mech* 37(8):2306–2312 (in Chinese)
- Yuan ZH, Ni WK, Tang C, Hu SM, J J G (2017) Experimental study of structure strength and strength attenuation of loess under wetting-drying cycle. *Rock Soil Mech* 38(7):1894–1902 (in Chinese)